Rupture Histories of Strong Earthquakes

Agalos A (1), Papadimitriou P (2), Makropoulos K (3)

(1) University of Athens, Department of Geophysics and Geothermics, Panepistimiopolis, Zographou, Athens, Greece, email aagalos@geol.uoa.gr
(2) University of Athens, Department of Geophysics and Geothermics, Panepistimiopolis, Zographou, Athens, Greece, email ppapadim@geol.uoa.gr
(3) University of Athens, Department of Geophysics and Geothermics, Panepistimiopolis, Zographou, Athens, Greece, email kmacrop@geol.uoa.gr

Keywords: rupture histories, slip models

Introduction

Digital broadband teleseismic records of P and *SH* waves are used to invert for rupture histories of recent strong earthquakes worldwide. In addition the strongest earthquakes that occurred in Greece from 1995 are also studied. The waveform data usually filtered between 0.01 to 1 Hz are used in a finite-fault inversion technique to determine the source complexities. The rupture history describes the slip distribution as a function of position and time on the fault. The advantage of using broadband records at teleseismic distances is that strong motion data are not always available or are frequently absent.

The followed finite-fault inversion approach does not permit the rupture velocity to change but the use of multiple time windows permits the same subfault to rupture multiple times. A linear least squares approach like the one followed gives a similar solution to a global search algorithm where the velocity can change relative to the position on the fault. The followed inversion approach permits the rake of the earthquake to vary upon the fault.

In cases where it is difficult to distinguish the rupture plane between the two nodal planes, the inversion procedure was applied twice. For the same set of parameters, the nodal plane which corresponds to the rupture plane, in most cases permits better fit between data and synthetics. The calculated rupture histories show the source complexity and directivity of the studied earthquakes. Slip models are calculated for several earthquakes in order to compute detailed static stress changes and synthetic peak ground velocity maps. In this study the results for two recent events are presented. These are the 2006 Kythira (Greece) earthquake and the 2007 Chile earthquake.

Data Used and Inversion Method followed

The last few years many studies have revealed the importance of the finite fault inversion procedure to our understanding of the earthquake rupture process which is able to provide an accurate spatial and temporal evolution of the coseismic slip on the ruptured fault. The finite fault inversion technique (Hartzell and Heaton 1983, Hartzell and Langer 1993, Hartzell et al., 1996, Mendoza and Hartzell 1999, Segikuchi and Iwata, 2002, Ji et al., 2002, Yagi et al., 2004) has been applied using teleseismically recorded waveforms or strong motion data. Several source inversion procedures that used teleseismic waveforms provided similar slip models using also other types of data such as geodetic (Wald and Heaton, 1994).

An inversion approach is applied for P and SH broadband waveforms at teleseismic distances between 30° and 90° from the earthquake epicenter. The stations belong to the Global Digital

Seismograph Network and are downloaded through the IRIS Data Management Center. The selection of the stations permitted the best possible azimuthal coverage which is always needed in this kind of inversion procedures. The teleseismic waveforms are instrument response corrected, integrated to displacement, band – pass filtered from 0.01 to 1 Hz using a Butterworth filter and re-sampled to 0.2 samples per second.

The finite fault inversion method followed developed by Hartzell and Heaton, (1983), is capable of estimating the spatial distribution of slip and risetime distribution on the ruptured fault. The application of this method starts by constructing a rectangular fault plane which is discretized to a number of uniform cells which are called subfaults. The source parameters (strike, dip, rake and source depth) are used as input to produce the elementary synthetics for each subfault. A total of 10 point sources were distributed over each subfault. The point sources are necessary to simulate a continuous rupture.

For every earthquake several different values of source velocity, varying from 2.6 to 3.5 km/sec, risetime, fault dimensions and time lag were used. The source of the elementary synthetics is of trapezoidal shape. The width of the source is chosen to be short compared to the total risetime on the fault. In most of the studied earthquakes the crust models used to produce the synthetics interpolated from the code CRUST2 (Bassin et al., 2000). The amount of slip in successive time intervals for each subfault is lagged in time by the width of the source. In this way, as described by Hartzell and Langer (1993), risetime functions are constructed and are free to vary as a function of position on the fault plane. The subfault may fail within the maximum allowed time window. The final rise time is obtained by the summation of the individual rise time functions for each time window. In most of the finite fault inversion studies the source velocity is taken as the 80 or 90% of the median S wave velocity.

The point source responses were computed with a code based on the generalized ray theory (Langston and Helmberger, 1975). The exact way these synthetics were constructed was discussed in the study of Heaton (1982), assuming that circular rupture fronts propagate at a given rupture velocity everywhere on the assumed fault plane. The absolute size of dislocation is specified to be related to the position on the fault. The elementary synthetics are always filtered with the same filter as the data and are convolved with an attenuation operation assuming t*=1 sec for P and t*=4 sec for SH waves.

In the finite fault inversion some trials are also made with the rake to vary across the dimensions of the fault, as it is used by Hartzell et al. (1996). In this case each subfault has n*2 model parameters to change during the inversion, where n is the number of time windows and 2 is for two mechanisms. The multiple time window approach of Hartzell and Heaton (1983) allows each subfault to rupture in any of the time windows used, based on the detail of the waveforms.

The observed waveforms and the synthetics produce an overdetermined system of linear equations of the form, **Ax=B**, where **A** and **b** are matrices concerning the joined elementary synthetics and teleseismic waveforms respectively, **x** is the solution vector including dislocation weights to be given at each subfault so that the final synthetics fit well the original data. The solution revealed from these matrices is not always stable and several constraints are needed. The constraints usually used at this kind of studies are well analyzed and explained in the studies of Hartzell and Heaton (1983) and Hartzell et al. (1991). Usually two constraints are used the moment minimization and smoothing.

In cases where there is no information about the rupture plane, the calculations are made twice using the two nodal planes of the focal mechanism. The nodal plane which is also the rupture plane, for the same parameters with the other plane used, would permit better fit between data and synthetics, as it is discussed by Mori and Hartzell (1990).

In conclusion the inversion method followed permits the identification of the fault plane, the calculation of the moment magnitude, the source time function, the fault dimensions and the detailed temporal and spatial position of slip on the fault.

Slip model of January 2006 Kythira, Greece earthquake and static stress transfer

On 8 January 2006 at 11:34 UTC a strong, thrust type faulting, earthquake (M_w=6.6) occurred in Southern Greece. The mainshock was located at 36.232°N, 23.395°E at the depth of 64 km. The data include 25 teleseismic P waveforms and 5 SH, of 60 sec duration, which were selected based upon data quality and azimuthal distribution. The waveforms were first converted to displacement by removing the instrument response and then used to constrain the slip history based on the linear finite fault inverse algorithm of Hartzell and Heaton (1983).

A surface of 70 km length and 24 km width was discretized by 108 subfaults, 18 along strike and 6 along dip. The surface edge of the fault starts at 48 km depth from the Earth surface and the down deep edge is at 72 km depth, the hypocenter is situated at 64 km depth and at a distance of 35 km from the left edge of the fault. Several rupture front velocities were tested. The fixed velocity value for rupture propagation of 3 km/sec produced the best fit between data and synthetics. The rake was left to change during the inversion between 70º and 160º, 6 time windows with 0.7 sec time lag duration for each one were used.

The fit between data and the calculated synthetics is presented in figure 1. The results show that the mainshock's moment magnitude is Mo=1*10^{26} dyne*cm, Mw=6.6 and the event ruptured a fault of nearly 30 km length. The nodal plane dipping southeast fits better the synthetics. The total duration of the mainshock is nearly 14 sec, with the majority of slip occurring between 3 and 8 sec of the far-field source time function. The inversion revealed one main region with significant slip. This region with significant slip is situated near the event's hypocenter with a maximum of 0.8 m slip, as presented in figure 2. The rake upon the fault mainly changes between 90º and 140º.

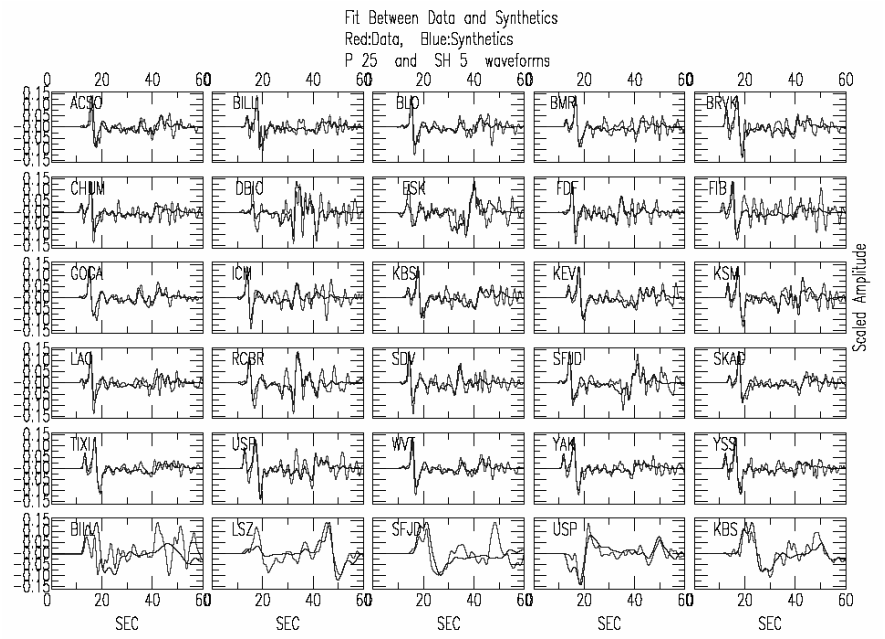

Figure 1. Comparison of observed and synthetic teleseismic waveforms. Synthetic to observed amplitude waveforms are indicated.

The slip model distribution revealed from the finite fault inversion procedure was used to compute the coseismic Static Coulomb Stress Changes in elastic half space. As it is presented from King et al. (1994); Harris and Simpson (2002), positive stress changes of 0.5

bars are able to trigger nearby events and negative values of the same amount are able to suppress them. Recent studies have revealed also stress transfer related with strong events occurred in Greece (Papadimitriou E., 2002, Ganas et al., 2006, Papadimitriou P. et al., 2006).

Earthquake induced stress changes, which are applied to a fault plane, are estimated using rectangular dislocation calculations that simulate static earthquake slip in an elastic halfspace (Okada, 1992). This technique is performed using the change of the Coulomb Failure Stress ΔCFS, (Harris and Simpson, 2002):

$$\Delta CFS = \Delta\tau + \mu(\Delta\sigma + \Delta p)$$

where $\Delta\tau$ is the change in shear stress on the failure plane in the expected rake direction on the target fault, μ is the coefficient of friction, $\Delta\sigma$ is the change of normal stress (positive for tension) and Δp is the change in pore fluid pressure. The value for the internal coefficient of friction used was μ=0.6 which is an intermediate value for Coulomb studies. For this calculation μ is considered constant and it is assumed not to change as a function of slip and time on the rupture plane. Robert's Simpson DLC software is used which is based on subroutines of Okada (1992) to calculate the displacements and their derivatives using Poisson's ratio 0.25 and a shear modulus of 0.33 Mbars.

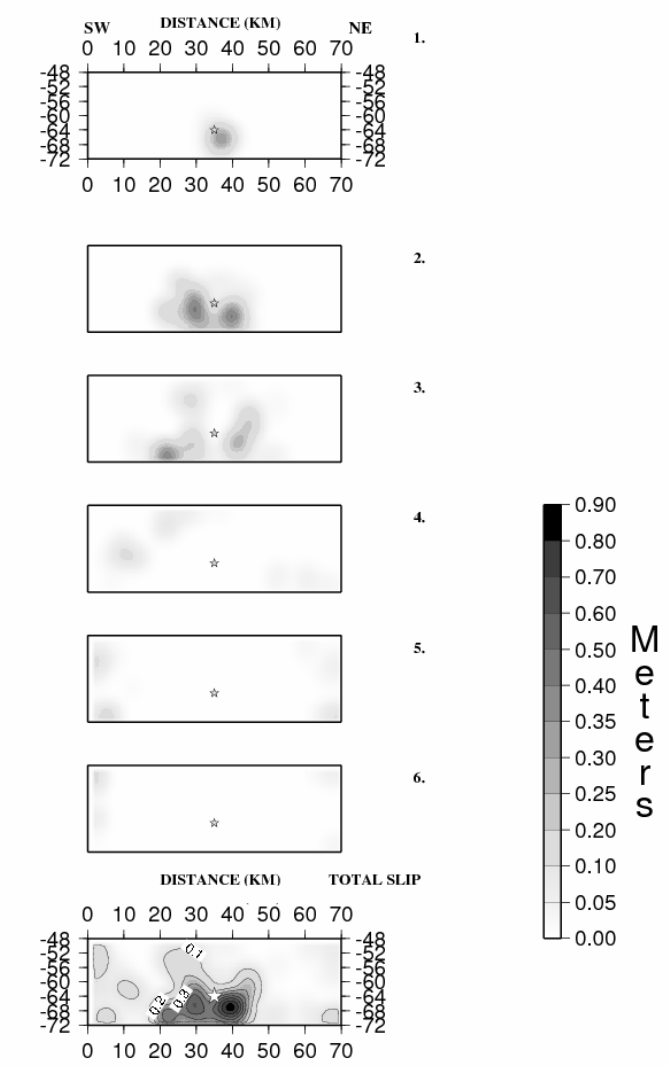

Figure 2. Temporal and Spatial Slip distribution on the ruptured fault plane. The first 6 sub-figures are snapshots with 3 seconds time difference between them. The seventh sub-figure presents the total slip on the ruptured fault.

In most of the papers studying the static stress changes uniform slip is usually adopted across the ruptured fault and most often the epicenter is selected to be in the center of the theoretical fault rupture. This assumption does not always provide any detail on calculations. In figure 3 it is showed the distribution of stress changes based on the suggested slip model of this study. The strongest static changes are concentrated in regions in the east of Kythira Island, mostly southern the fault rupture. The obtained Coulomb stress pattern indicates positive values of stress in the direction where the Leonidio earthquake occurred in January of 2008, but it is not clear that it was triggered by the Kythira event because of the very low values of transferred stress.

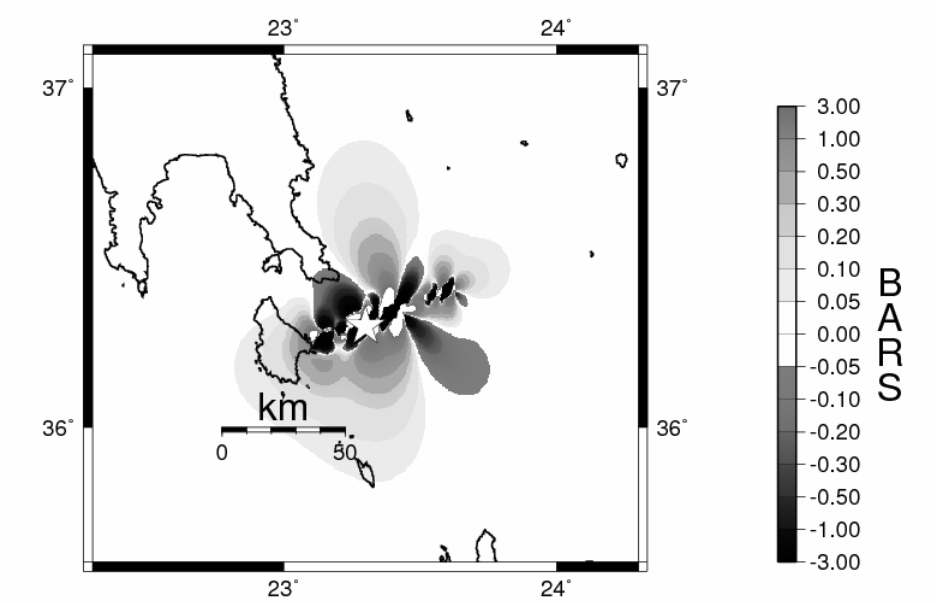

Figure 3. Calculated coseismic static stress changes for Kythira earthquake using the slip model revealed from the finite fault inversion procedure. White star represents the epicenter of the mainshock.

Slip model of November 2007 Chile earthquake and Synthetic PGV map

On 14 November at 15:40:50 UTC a very strong, thrust type faulting, earthquake (M_w=7.7) occurred in Chile. The rupture process and history are studied using broadband teleseismic data. The mainshock was located by USGS at 22.204°S, 69.869°W and EMSC at 22.17°S, 69.97°W about 165 km NNE of Antofagasta, Chile. The data include 12 teleseismic P waveforms and 12 SH waveforms which were selected based upon data quality and azimuthal distribution. These waveforms were first converted to displacement by removing the instrument response and then used to constrain the slip history based on the linear finite fault inverse algorithm of Hartzell and Heaton (1983). The broadband teleseismic data, downloaded through Iris Wilber II application, were inverted by allowing a variable dislocation rise time at each point on the fault. A surface of 180 km length and 30 km width was discretized by 108 subfaults, 18 along strike and 6 along dip. The surface edge of the fault is at 20 km depth and the down deep edge at 50 km depth, the hypocenter is situated at 37 km depth and at a distance of 120 km from the left edge of the fault. Several rupture front velocities were tested. The fixed velocity value for rupture propagation of 2.6 km/sec produced the best fit between data and synthetics. The velocity model used to produce the elementary synthetics is provided by Mendoza et al. (1994) who studied another strong event in Chile.

The results show that the moment magnitude of the mainshock is, Mo=5*10^{27}dyne*cm, Mw=7.7 and the event ruptured a fault of nearly 120 km length. The nodal plane dipping-west fits the data better. The total duration of the mainshock is 56 sec, with the majority of slip occurring the first 40 sec of the far-field source time function. The inversion revealed two main regions with significant slip (figure 4). The first region, at the northern part of the fault, extends around the earthquake's hypocenter and the second which has two maximum peaks is found at the southern part of the fault nearly 40 km from the first region. In the finite fault inversion 6 time windows with 2 sec time lag duration for each one were used. The rake which was left to vary during the inversion approach between 90° and 180° mainly varied between 90° – 100°. Figure 5 shows the Peak Ground Velocity distribution using the calculated slip model and the code of Bouchon (1981).

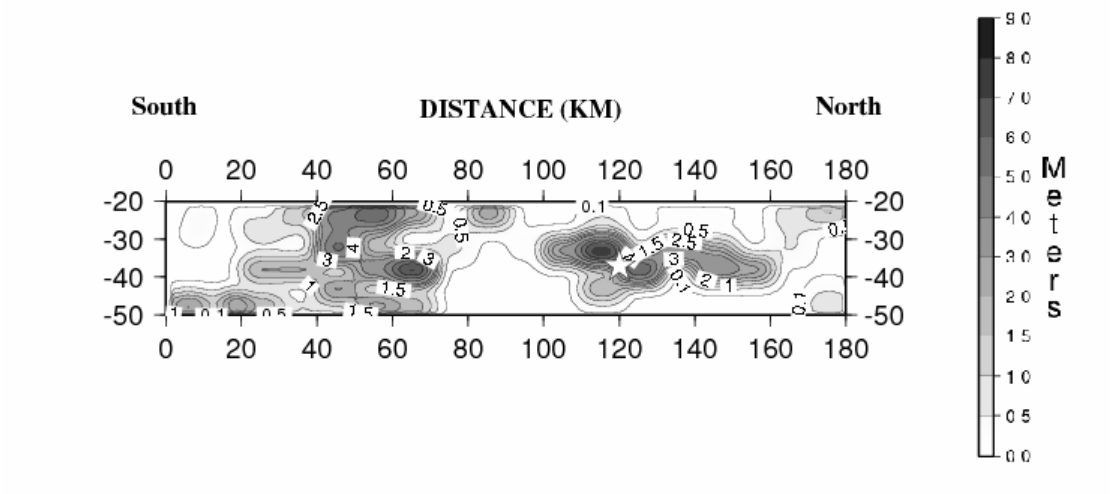

Figure 4. Slip distribution on the ruptured fault plane for 2007 Chile earthquake.

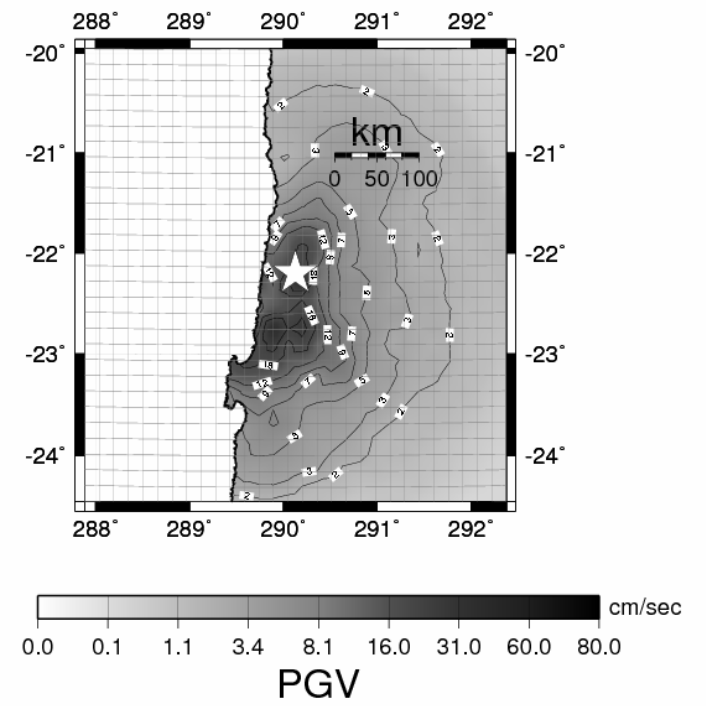

Figure 5. Synthetic Peak Ground Velocity map estimated using the slip model retrieved by the waveform inversion. The white star indicates the earthquake's epicenter.

Conclusions

In this study two detailed coseismic slip models are presented for the January of 2006 Kythira, Greece earthquake and the 2007 Chile earthquake. Both earthquakes are related with thrust type faulting. The inversion approach applied revealed the spatial and temporal distribution of slip. The slip model of Kythira earthquake is quit simple. The dimension of the ruptured fault is about 30x10 km with a maximum slip of 0.8 m close to 68 km depth. Static Coulomb stress analysis, using the calculated slip model, did not reveal clearly stress transfer to the Leonidio earthquake occurred two years after.

The slip distribution of Chile earthquake is complex with at least two sources. The dimension of the ruptured fault is about 120x15 km with a maximum slip of 7 m close to 35 km depth. The determined slip model is used to calculate the spatial distribution of the peak ground velocity (PGV). The strongest values of PGV are concentrated in two regions which can be related with the two revealed main sources.

Acknowledgments

We would like to thank Dr. Stephen Hartzell for explaining and providing the finite fault inversion codes used in this study, Robert Simpson for providing the code that used to compute the static stress changes. Most of figures were made using the GMT software (Wessel and Smith, 1981).

References

Bassin C, Laske G & Masters G (2000). The Current Limits of Resolution for Surface Wave Tomography in North America, *EOS Trans AGU, 81, F897.*

Bouchon M (1981). A simple method to calculate Green's functions for elastic layered media, *BSSA, 71, 4, 959-971.*

Ganas A., Sokos E., Agalos A., Leontakianakos G., Pavlides S (2006). Coulomb stress triggering of earthquakes along the Atalanti Fault, central Greece: Two April 1894 M6+ events and stress change patterns, *Tectonophysics, 420, 357-369.*

Harris R. A. & Simpson R. W (2002). The 1999 MW 7.1 Hector Mine, California Earthquake - A test of the stress shadow hypothesis?, *BSSA, 92, 4, 1497-1512.*

Hartzell S. H. & Heaton T. H (1983). Inversion of strong ground motion and teleseismic waveform data for the fault rupture history of the 1979 Imperial Valley, California, earthquake, *BSSA, 73, 1553-1583.*

Hartzell H., Stephen, Stewart S. Gordon & Mendoza C (1991). Comparison of L1 and L2 norms in a teleseismic waveform inversion for the slip history of the Loma Prieta, California, earthquake, *BSSA, 81, 1518-1539.*

Hartzell H., Stephen & Langer C (1993). Importance of Model Parameterization in Finite Fault Inversions: Application to the 1974 Mw 8.0 Peru Earthquake, *JGR, 98, B12, 22123-22134.*

Hartzell H., Stephen, Pengcheng, Liu & Mendoza C (1996). The 1994 Northridge, California earthquake: investigation of rupture velocity, risetime and high-frequency radiation, *J.G.R, 101, 20091-20108.*

Heaton T. H. (1982). The 1971 San Fernando earthquake: a double event?, *BSSA, 72, 2037-2062.*

Ji C., Wald D. J., & Helmberger D. V (2002). Source description of the 1999 Hector Mine, California earthquake; Part I: Wavelet domain inversion theory and resolution analysis, *Bull. Seism. Soc. Am., Vol 92, 4, 1192-1207.*

King G. C. P., Stein R. S., & Lin. J (1994). Static Stress changes and the triggering of earthquakes, *BSSA, 84, 935-953.*

Langston C. A. & Helmberger D. V (1975). A procedure for modeling shallow dislocation sources, *Geophys. J. Roy. Astr. Soc., 42, 117-130.*

Mendoza C. & Hartzell S (1999). Fault-slip distribution of the 1995 Colima-Jalisco, Mexico,Earthquake, *BSSA, 89, 5, 1338-1344.*

Mori, Jim & Hartzell S (1990). Source inversion of the 1988 Upland, California, earthquake: determination of a fault plane for a small event, *BSSA, 80, 507-517.*

Okada, Y (1992). Internal deformation due to shear and tensile faults in a half-space, *BSSA, 82, 1018-1040.*

Sekiguchi H. & Iwata T (2002). Rupture process of the 1999 Koaceli, Turkey, earthquake estimated form strong-motion waveforms, *BSSA, 92, 300-311.*

Papadimitriou E (2002). Mode of Strong Earthquake Recurrence in the Central Ionian Islands (Greece): Possible Triggering due to Coulomb Stress Changes Generated by the Occurrence of Previous Strong Shocks, *Bulletin of the Seismological Society of America, 92, 8, 3293-3308.*

Papadimitriou P., Kaviris G., Makropoulos K (2006). The Mw=6.3 2003 Lefkada earthquake (Greece) and induces stress transfer changes, *Tectonophysics, 423, 73-82.*

Wald D. J. & Heaton T. H (1994). Spatial and temporal distribution of slip for the 1992 Landers, California, earthquake*, BSSA, 84, 3, 668-691.*

Wessel P. & Smith W. H. F (1991). Free software helps map and display data, *EOS Trans. AGU, 72, 441.*

Yagi, Yugi, Mikumo, Takeshi, Pacheco, Chavier, & Reyes G (2004). Source Rupture Process of the Tecoma´n, Colima, Mexico Earthquake of 22 January 2003, Determined by Joint Inversion of Teleseismic Body-Wave and Near-Source Data, *BSSA, 94, 5, 1795-1807.*